Static and Kinetic Studies of Complex Formations between Calmodulin and MastoparanX

Tomohiko Murase and Takayoshi Iio*

Physics Section, Division of Material Science, Graduate School of Science, Nagoya University, Chikusa-ku, Nagoya, Aichi, 464-8602, Japan

Received September 11, 2001; Revised Manuscript Received November 19, 2001

ABSTRACT: Ca^{2+}-induced complex formation between calmodulin (CaM) and mastoparanX (MasX) was studied by a fluorescence spectroscopy and by a stopped-flow method. The measurements of the fluorescence anisotropy in the presence of calcium and the fluorescence titration with Ca^{2+} revealed that the N- and C-domains of CaM bound cooperatively MasX, while the tryptic fragments of CaM (TR_1C, 1−77 and TR_2C, 78−148) bound independently MasX. The Trp-fluorescence stopped-flow experiments revealed that the Ca^{2+}-induced binding of CaM and MasX was composed of two processes: one was a rapid binding of the N-domain of CaM to MasX, which was induced by the rapid Ca^{2+} binding to the N-sites of CaM. The other was a slow biphasic process. Its fast phase was the binding of the C-domain of CaM to MasX, which was induced by the slow Ca^{2+} binding to the C-sites. Interestingly, the kinetics of the slow process varied with the Ca^{2+} concentrations. At the low Ca^{2+} concentrations, its rate constant increased to around 20 s^{-1} as the Ca^{2+} concentration increased. At the high Ca^{2+} concentrations, the Ca^{2+}-induced binding of the C-domain of CaM to MasX proceeded at a constant rate around 20 s^{-1}. This suggested an existence of a rate-limiting step for the Ca^{2+}-induced binding of the C-domain of CaM to MasX at the high Ca^{2+} concentrations. The slow phase of the slow process may be a rearrangement of the CaM−MasX complex. These results led to our model of a molecular kinetic mechanism of the Ca^{2+}-induced complex formation between CaM and MasX.

Calmodulin (CaM)[1] is a Ca^{2+}-binding protein in all eukaryotic cells (*1*). The physiological role of CaM is a Ca^{2+}-dependent modulator in the cell (*1, 2*). When the cell accepts the external stimuli, cytoplasmic Ca^{2+} concentration rises by either or both the release of Ca^{2+} from internal stores and the influx of extracellular Ca^{2+} (*3*−*7*). Over a certain Ca^{2+} concentration, CaM binds Ca^{2+} and changes its conformation. Through this conformational change, CaM associates with or dissociates from many CaM-dependent target proteins and peptides, and regulates their physiological functions (*7*−*11*). Such sequential events are observed in the wide range of physiological phenomena (*7, 12*−*20*).

CaM has a dumbbell structure with two similar domains connected by a central helix (Phe 65 to Phe 92) (*21*). Each domain has two Ca^{2+}-binding sites (*22*), which is composed of a helix−loop−helix structure called an EF-hand motif (*23*). Ca^{2+} binding to the sites induces the exposure of hydrophobic residues of CaM comprising the binding sites for target proteins and peptides. Many CaM-dependent target proteins and peptides have basic and hydrophobic residues as a common feature of the CaM-binding site (*24, 25*). Some structures of the CaM−target peptide complexes in the presence of calcium were solved by X-ray crystallography and nuclear magnetic resonance methods. In the complexes, Ca^{2+}-bound CaM takes a jack-knifed shape, in which the flexible central linker of CaM (Arg 74 to Glu 82) is bent to surround the peptide which assumes the α-helical conformation. Several types of arrangements have been reported for complexes of CaM and target peptides. One of them is an antiparallel arrangement in which the N- and C-domains of CaM interact with the C- and N-terminals of target peptide, respectively (*26*−*28*); another is a parallel one with the reverse location of the domains of CaM in the complex (*29*). In addition, the other structures have been recently reported (*30*−*34*). Moreover, it is reported that even at low calcium concentrations CaM interacts with some target proteins and peptides (*13, 35*−*37*). For instance, Hill et al. reported that apoCaM interacts with a peptide derived from myosin light chain kinase (MLCK peptide) by electrostatic forces between the charged residues within CaM and the MLCK peptide (*36*).

Many research groups have been interested in the molecular mechanism of the complex formation of CaM with target proteins and peptides. Static and kinetic studies of the complex formation have been performed by using fluorescence spectroscopy, calorimetry, nuclear magnetic resonance, stopped-flow, temperature jump, and other methods. In particular, many kinetic studies of the dissociation of Ca^{2+} from Ca^{2+}-bound CaM and Ca^{2+}-bound CaM complex with

* To whom correspondence should be addressed. Telephone: + 81-52-789-2434. Fax: +81-52-789-2436. E-mail: j45694a@nucc.cc.nagoya-u.ac.jp.

[1] Abbreviations: CaM, bovine brain calmodulin; MasX, mastoparanX; TR_1C, tryptic fragment comprising residues 1−77 of bovine brain calmodulin; TR_2C, tryptic fragment comprising residues 78−148 of bovine brain calmodulin; MLCK, myosin light chain kinase; EGTA, ethylene glycol bis(β-aminoethyl ether)-*N*,*N*,*N*′,*N*′-tetraacetic acid; MOPS, 3-(*N*-morpholino)propanesulfonic acid.

10.1021/bi011782r CCC: $22.00
Published on Web 01/09/2002

target peptide revealed interesting features of CaM and CaM−target peptide complexes (*38*−*49*).

It has been established that the calcium dissociation constant (Kd_{Ca}) of the C-domain of CaM is 2- or 3-fold lower than that of the N-domain (*50*, *51*). Kinetic studies established that the rate constant (k_{off}) for the dissociation of Ca^{2+} from the N-domain of CaM is approximately 100-fold higher than that of the C-domain (*39*−*41*, *44*, *47*). On the basis of these results, the rate constant (k_{on}) for the Ca^{2+} binding of each domain of CaM is calculated from k_{off}/Kd_{Ca}. The k_{on} value for the binding of Ca^{2+} to the N-domain of CaM is approximately 30−50-fold higher than that of the C-domain (*44*). These results allow us to recognize the feature of each domain of CaM for Ca^{2+}; the C-domain of CaM binds Ca^{2+} strongly, and the N-domain responds rapidly to the change of the Ca^{2+} concentration around CaM. With these properties of CaM, several models of the interaction between CaM and target peptide have so far been proposed (*46*−*49*, *52*).

In contrast to these studies, little is known about the kinetics of the Ca^{2+}-induced complex formation between CaM and target peptide. Our research aims to reveal the kinetic process of the complex formation; especially we are interested in revealing how each part of CaM interacts with target peptide and in what role each part plays. We adopted, as a target peptide, mastoparanX (MasX). MasX is a 14 residue peptide from the venom of wasp, whose amino acid sequence is INWKGIAAMAKKLL-NH_2 (*53*, *54*). MasX causes the degranulation of mast cell. It also activates GTP-binding regulatory proteins (*55*, *56*). Many groups have reported that MasX binds to CaM (*47*, *57*−*64*), and it is known that MasX in the globular CaM−MasX complex assumes an α-helical structure (*59*, *61*, *63*). In this study, we used three experimental methods: fluorescence anisotropy measurement, fluorescence titration method, and mainly stopped-flow method for the study of the Ca^{2+}-induced complex formation between apoCaM or apoCaM tryptic fragment(s) (apoTR_1C, apoTR_2C, or both) and MasX. On the basis of our results, we constructed a scheme for the molecular kinetic mechanism of the Ca^{2+}-induced complex formation between CaM and MasX.

MATERIALS AND METHODS

Materials. CaM was extracted from bovine brain and purified as described previously by Itakura and Iio (*65*). The purity of the protein was checked by 15% SDS−polyacrylamide gel electrophoresis. The concentration of CaM was determined using $A_{1mg/mL,276nm} = 0.18$ (*66*) and a molecular weight of 16 700 (*67*). Tryptic fragments of CaM, TR_1C (fragment 1−77) and TR_2C (fragment 78−148), were obtained, and the purity of the fragment was checked according to the procedure described previously by Itakura and Iio (*65*). MasX was purchased from BACHEM AG (Bubendorf, Switzerland). Pure solutions of 1 M $CaCl_2$ and EGTA were purchased from Shinyo Pure Chemicals Co., Ltd. (Osaka, Japan), and Dojindo (Kumamoto, Japan), respectively.

Removal of Calcium Contamination. Removal of calcium contamination is necessary in this study. We removed the calcium contamination by the following method. All labwares and flow passages within the stopped-flow spectrofluorometer were successively washed with buffer A (5 mM EGTA, 0.1 M KCl, and 50 mM MOPS, pH 7.00), buffer B (10 μM EGTA, 0.1 M KCl, and 50 mM MOPS, pH 7.00), and ultrapure water (from Milli-Q apparatus, Millipor, Inc.).

Preparation of Ca^{2+}-Free Protein and Peptide. We prepared Ca^{2+}-free protein and peptide by gel chromatography on Sephadex G-25. At first, the column was equilibrated with buffer B. Then an aliquot of buffer A (2−3 mL) and a solution containing protein or peptide (4−5 mL) were successively applied to a Sephadex G-25 column. Then Ca^{2+}-free protein or peptide fraction was collected using buffer B as the eluant.

Fluorescence Measurements. Fluorescence anisotropy and fluorescence emission spectra were measured with a Hitachi F-4500 fluorescence spectrophotometer. The fluorometer was connected to a water bath to maintain a constant temperature (25 °C) of the samples. The buffer in the fluorescence experiments was 0.1 M KCl and 50 mM MOPS, pH 7.00.

Measurements of fluorescence anisotropy for Trp of MasX were performed with excitation at 295 nm (band-pass 2.5 nm) through a dichroic polarizer, and the average fluorescence intensities (I_{vv}, I_{vh}, I_{hv}, and I_{hh}) at 340 nm were monitored through a dichroic polarizer (band-pass 10 nm). The anisotropy (r) is calculated from the following equations:

$$r = \frac{I_{vv} - GI_{vh}}{I_{vv} + 2GI_{vh}} \quad (1)$$

$$G = I_{hv}/I_{hh} \quad (2)$$

where I_{vv} and I_{vh} are the intensities of the vertically and horizontally polarized fluorescence lights with vertically polarized excitation, respectively, and I_{hv} and I_{hh} are those with horizontally polarized excitation (*68*).

Measurements of fluorescence emission spectra for Trp of MasX were performed with excitation at 295 nm (band-pass 2.5 nm) and with the emission scanned from 300 to 450 nm (band-pass 2.5 nm). The fluorescence intensity of Trp at 330 nm was obtained by averaging at least two spectra. Free calcium ion concentration ($[Ca^{2+}]_{free}$) in solution was calculated from the concentrations of EGTA and $CaCl_2$ added to the solution using the numerical constants of Schwarzenbach et al. (*69*). For two-state transition curves, the curve-fitting of the fluorescence titration data was performed with a Hill equation as follows:

$$\frac{F - F_{min}}{F_{max} - F_{min}} = \frac{([Ca^{2+}]_{free})^n}{([Ca^{2+}]_{free})^n + (Kd_{Ca})^n} \quad (3)$$

$$pCa_{1/2} = -\log(Kd_{Ca}) \quad (4)$$

where F, F_{min}, F_{max}, and n are the fluorescence intensity, F at minimum, F at maximum, and Hill constant, respectively. The Kd_{Ca} is the calcium dissociation constant. The $pCa_{1/2}$ is the midpoint pCa value of the fluorescence titration curve. For the three-state transition curve, a sum of two Hill equations was used for the curve-fitting.

A Microsoft Excel Solver function was used for minimizing the error square sum for the curve-fitting of all data in anisotropy titration and calcium titration experiments, whose variances were less than 2.7×10^{-5} and 8.9×10^{-4}, respectively.

Stopped-Flow Measurements. Kinetic measurements were performed with an Applied Photophysics Ltd. (Leatherhead,

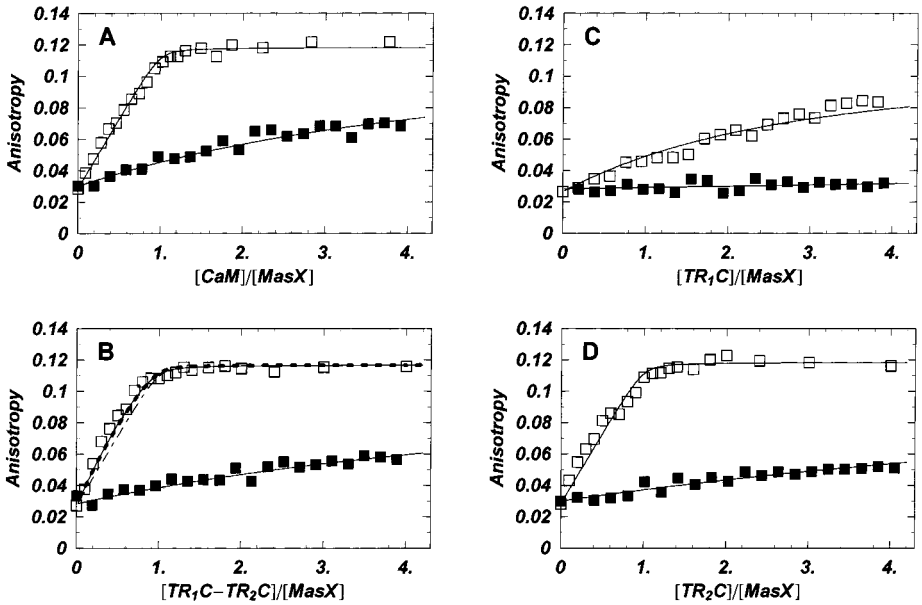

FIGURE 1: Fluorescence anisotropy titration of 5.0 μM MasX with (A) CaM, (B) equimolar mixture of TR_1C and TR_2C (TR_1C-TR_2C), (C) TR_1C, and (D) TR_2C. The open symbols designate the experimental data obtained in the solution containing 4 mM EGTA and 4.2 mM $CaCl_2$ (pCa 3.7); the closed symbols in 4 mM EGTA. All lines are calculated using the dissociation constants summarized in Table 1. The dash−dotted line of panel B is the anisotropy titration curve for the CaM system (from panel A). The dotted line of panel B is an anisotropy titration curve for independent binding of TR_1C and TR_2C with MasX. The solid line of panel B is for competitive binding of the fragments with MasX. Fluorescence anisotropy was measured at 340 nm emission wavelength (band-pass 10 nm) with excitation at 295 nm (band-pass 2.5 nm) in 0.1 M KCl and 50 mM MOPS, pH 7.00 at 25 °C.

U.K.) model SX.17 MV stopped-flow spectrofluorometer. The excitation monochromator was set to 290 nm (band-pass 11.6 nm), and the fluorescence emission of Trp was monitored through a 320 nm cutoff filter. Since the fluorescence intensity was observed through the cutoff filter, the degree of kinetic fluorescence intensity change for the stopped-flow experiment was different from that of the static fluorescence titration experiment. In particular, the TR_1C-MasX system showed a fluorescence decrease in the Ca^{2+}-induced MasX binding reaction to TR_1C, which was observed by the stopped-flow method. On the other hand, it showed a fluorescence increase in the static fluorescence titration experiment. The stopped-flow apparatus had a deadtime of 1.4 ms at a drive pressure of about 8 bar. The measurements were made in 0.1 M KCl and 50 mM MOPS, pH 7.00 at 10 °C. We obtained reaction curves by averaging at least four reaction traces. The curve-fitting program (by P. J. King, Applied Photophysics Ltd.) used the nonlinear Levenberg−Marquardt algorithm. The reaction traces after 1.5 ms were fitted with single to triple exponential curves in the range of variance $<7.2 \times 10^{-5}$.

Computer Simulations. Numerical simulations were performed by Mathematica (Wolfram Research, Inc.) using the following k_{on} and k_{off} values of the Ca^{2+}-binding sites of CaM and EGTA at 10 °C: $k_{on} = 1.7 \times 10^8$ M^{-1} s^{-1} and $k_{off} = 480$ s^{-1} for the N-sites of CaM (*70*); 5.3×10^6 M^{-1} s^{-1} and 3.5 s^{-1} for the C-sites (*70*); 1.3×10^6 M^{-1} s^{-1} and 0.55 s^{-1} for EGTA (*44*). These k_{off} values of the N- and C-sites of CaM were determined by the stopped-flow method: a solution of 5 μM Ca^{2+}-bound CaM in 0.1 M KCl and 50 mM MOPS, pH 7.00, was mixed with a solution of the calcium chelator Quin 2 (100, 200, or 300 μM), and the Quin 2 fluorescence change was observed to determine the k_{off} values. The k_{off} values were similar to those obtained by the same method for TR_1C and TR_2C (*39*−*41*, *44*). The Kd_{Ca} values were obtained by the fluorescence titration method using 5 μM TR_1C and 5 μM TR_2C, respectively, in 0.1 M KCl, 50 mM MOPS, pH 7.00, and 50 μM 2-*p*-toluidinylnaphthalene sulfonate (purchased from Sigma). These Kd_{Ca}s were similar to those reported by Johnson et al. (*44*). The aforementioned k_{on} values were calculated from k_{off}/Kd_{Ca}.

RESULTS

Fluorescence Anisotropy Measurements. The fluorescence anisotropy depends on the rotational freedom of the chromophore, which is influenced by its environment. MasX has a Trp residue at the third position, but CaM has no Trp residue. We can determine the degree of complex formation of CaM or CaM fragment(s) with MasX by measuring the fluorescence anisotropy of the Trp residue. MasX was titrated with CaM or CaM fragment(s) in the presence and the absence of calcium, and Trp-fluorescence anisotropy was measured. These anisotropy titration curves are shown in Figure 1.

We determined the *K*d value of the protein−MasX complex by curve-fitting of the experimental titration data shown in Figure 1 (variance $<2.7 \times 10^{-5}$). The *K*d values are listed in Table 1. In the presence of calcium, titration curves for CaM and TR_2C showed saturation at a 1:1 molar ratio of protein/MasX (Figure 1, panels A and D). This means that CaM and TR_2C form a 1:1 complex with MasX, respectively. The titration curve for an equimolar mixture of TR_1C and TR_2C showed a steep increase at low molar ratio of fragments/MasX and leveled off at a 1:1 molar ratio (Figure 1, panel B). The TR_1C system showed no saturation of the anisotropy titration, indicating that TR_1C bound more weakly to MasX than the others (Figure 1, panel C).

In the absence of calcium, titration curves for CaM, TR_2C, and TR_1C-TR_2C showed no saturation in the fluorescence

Table 1: Dissociation Constants (*K*d) of MasX and CaM or CaM Fragment(s) Obtained by Fluorescence Anisotropy Measurements[a]

system	*K*d (M)	
	$-Ca^{2+}$ [b]	$+Ca^{2+}$ [c]
CaM	2.19×10^{-5} [e]	$(3.33 \pm 0.95) \times 10^{-8}$
TR_1C	5.25×10^{-4} [f]	1.03×10^{-5} [f]
TR_2C	5.71×10^{-5} [e]	$(3.58 \pm 0.34) \times 10^{-8}$
TR_1C-TR_2C[d]	3.54×10^{-5} [e]	1.03×10^{-5} [g,h] 3.58×10^{-8} [g,i]

[a] In 0.1 M KCl and 50 mM MOPS, pH 7.00 at 25 °C. [b] In the presence of 4 mM EGTA. [c] In the presence of 4 mM EGTA and 4.2 mM $CaCl_2$ (pCa 3.7). [d] TR_1C-TR_2C represents an equimolar mixture of TR_1C and TR_2C. [e] We assumed that the level-off anisotropy of each complex in the absence of calcium was the same as that in the presence of calcium. [f] We assumed that the level-off anisotropy of the TR_1C-MasX complex is the arithmetic mean of those for CaM, TR_2C, and TR_1C-TR_2C systems ($r = 0.113$). [g] We assumed that TR_1C and TR_2C bound independently to MasX (see text). [h] For TR_1C-MasX. [i] For TR_2C-MasX.

anisotropy titration. The titration curve for TR_1C showed little change of the anisotropy. These results indicate that apoCaM, apoTR_2C, and apoTR_1C-apoTR_2C bind weakly to MasX, while there is little binding of apoTR_1C to MasX.

Since we could not determine the level-off anisotropy values in the absence of calcium, we assumed here that the level-off anisotropy of each complex in the absence of calcium was the same as that in the presence of calcium. We also assumed that the level-off anisotropy of the TR_1C-MasX complex is the arithmetic mean of those for the CaM, TR_2C, and TR_1C-TR_2C systems ($r = 0.113$).

Calcium Titration of CaM or CaM Fragment(*s*) *and MasX Systems*. The Trp residue of MasX changes its fluorescence spectrum upon complex formation with CaM or CaM fragment(s). We carried out the titration of an equimolar mixture of CaM or CaM fragment(s) and MasX with calcium by measuring the Trp-fluorescence intensity change and the shift of the Trp emission peak of MasX. Titration curves of Figure 2 showed that fragment(s) and MasX systems underwent a two-state transition. Midpoints ($pCa_{1/2}$) of the titration curves for these systems were determined by the curve-fitting analyses of the experimental data (variance $< 8.9 \times 10^{-4}$), and were listed in Table 2. The $pCa_{1/2}$ of the TR_2C-MasX system was higher than that of the TR_1C-MasX system. This means that the TR_2C-MasX system binds Ca^{2+} more strongly than the TR_1C-MasX system. The titration curve of the CaM−MasX system resulted in a three-state transition. Since the C-domain sites bind Ca^{2+} more strongly than the N-domain sites, the first transition at the high-pCa region is due to the Ca^{2+} binding to the C-domain, thereby causing the Ca^{2+}-bound C-domain of CaM to bind to MasX. The second transition at the low-pCa region is due to the Ca^{2+} binding to the N-domain, thus forming the final CaM−MasX complex in which both the Ca^{2+}-bound domains bind to MasX. Malencik and Anderson reported the same transition curve for the CaM−MasX system as ours (*60*). On the other hand, an equimolar system of TR_1C, TR_2C, and MasX showed a two-state transition. The $pCa_{1/2}$ of this system was higher than those of the TR_1C-MasX and TR_2C-MasX systems.

The Trp chromophore of MasX showed the blue-shift of the Trp emission peak upon Ca^{2+}-induced complex formation between CaM or CaM fragment(s) and MasX. For instance,

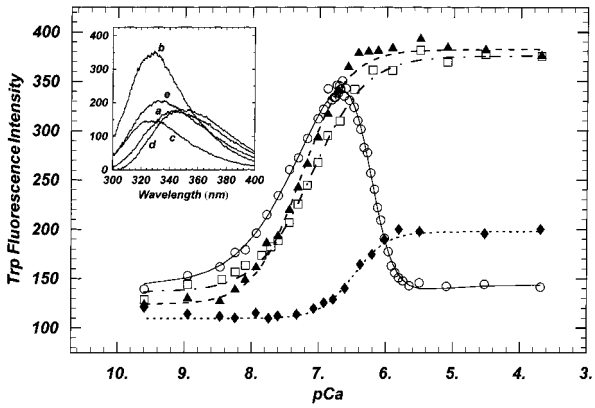

FIGURE 2: Fluorescence titration curves of CaM or CaM fragment(s) and MasX with $CaCl_2$. Trp-fluorescence of MasX (5.0 μM) in the presence of 5.0 μM CaM (○), 5.0 μM TR_1C (◆), 5.0 μM TR_2C (□), and a mixture of 5.0 μM TR_1C and 5.0 μM TR_2C (▲) is shown as a function of pCa. The lines represent best-curve fits to the data of the CaM−MasX system (solid line), the TR_1C-TR_2C-MasX system (dashed line), the TR_1C-MasX system (dotted line), and the TR_2C-MasX system (dash−dot−dashed line). Trp-fluorescence was monitored at 330 nm (band-pass 2.5 nm) with excitation at 295 nm (band-pass 2.5 nm) in 0.1 M KCl and 50 mM MOPS, pH 7.00 at 25 °C. The solution contained 4 mM EGTA, and its pCa was adjusted by adding $CaCl_2$. The inset shows the fluorescence spectra of the CaM−MasX system at (a) pCa 9.6, (b) pCa 6.7, and (c) pCa 3.7, and of the TR_1C-MasX system at (d) pCa 9.6 and (e) pCa 3.7.

Table 2: Midpoints ($pCa_{1/2}$) and Hill Constants of the Fluorescence Titration Curves of CaM or CaM Fragment(s) and MasX Systems[a]

system	mole ratio	$pCa_{1/2}$	Hill constant
CaM−MasX	1:1	7.31 ± 0.12[b] 6.31 ± 0.08[c]	0.92 ± 0.04[b] 2.95 ± 0.59[c]
TR_1C-MasX	1:1	6.49 ± 0.01	1.60 ± 0.17
TR_2C-MasX	1:1	7.15 ± 0.04	1.10 ± 0.02
TR_1C-TR_2C-MasX	1:1	7.34 ± 0.06	1.21 ± 0.07

[a] In 0.1 M KCl, 50 mM MOPS, pH 7.00 at 25 °C. [b] A fluorescence increase phase. [c] A fluorescence decrease phase.

when the calcium concentration was increased from pCa 9.6 to pCa 3.7, the Trp emission peak of the CaM−MasX system shifted from about 350 nm to about 330 nm (inset of Figure 2). This result indicates that at the high calcium concentration the Trp residue of MasX is close to the hydrophobic part of each domain of CaM or the tryptic fragment(s) of CaM. In the absence of calcium, the Trp-fluorescence emission spectrum of the TR_1C-MasX system was the same as that of the free MasX, while the other systems showed little fluorescence intensity increase in the region lower than 350 nm (inset of Figure 2).

Stopped-Flow Studies of Ca^{2+}*-Induced Complex Formation of CaM or CaM Fragment*(*s*) *with MasX*. We performed the stopped-flow experiments to study the kinetics of the Ca^{2+}-induced binding of CaM or CaM fragment(s) to MasX. A solution containing apoCaM (10 μM), MasX (10 μM), and EGTA (10 μM) was mixed with a solution of calcium (CaM−MasX versus Ca^{2+} system), and the Ca^{2+}-induced complex formation was observed by following the Trp-fluorescence intensity change. The resultant stopped-flow traces depended on the calcium concentrations of the calcium solution as shown in Figure 3. The traces were classified into two patterns as follows: (i) When the molar ratio of calcium to CaM was less than or equal to 4 (low calcium

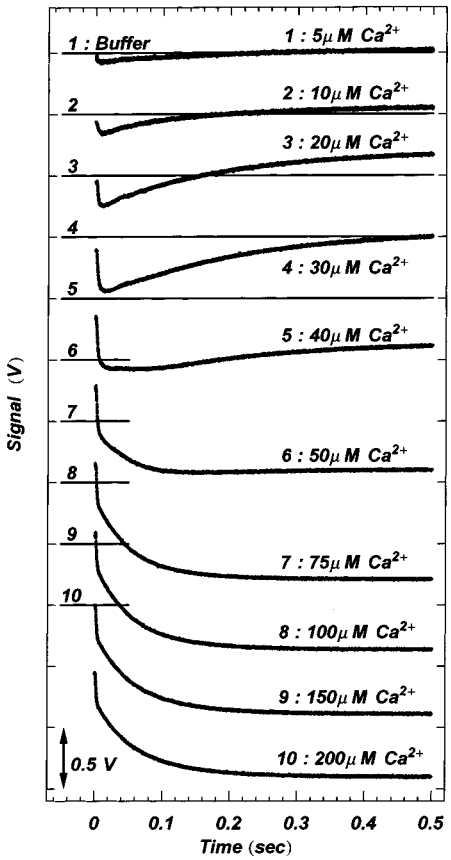

FIGURE 3: Stopped-flow traces for the Ca^{2+}-induced binding of CaM and MasX. A solution of 10 μM CaM, 10 μM MasX, and 10 μM EGTA was mixed with $CaCl_2$ solution, and the time-course of Trp-fluorescence intensity change was observed. Calcium concentrations of the $CaCl_2$ solutions are shown in the figure. Each horizontal solid line represents the initial level of each trace. The number of the line and the trace are on a pair. Trp-fluorescence was measured through a cutoff filter of 320 nm with an excitation light at 290 nm at 10 °C.

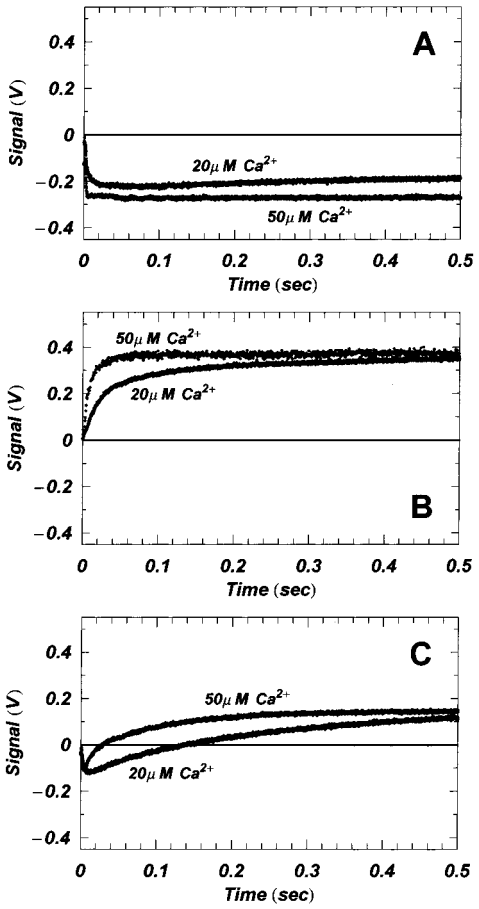

FIGURE 4: Stopped-flow traces for the Ca^{2+}-induced binding of CaM fragment(s) and MasX. Stopped-flow traces in each panel were obtained by the same method as in Figure 3. (A) A solution of 10 μM TR_1C, 10 μM MasX, and 10 μM EGTA was mixed with $CaCl_2$; (B) 10 μM TR_2C, 10 μM MasX, and 10 μM EGTA was mixed with $CaCl_2$; (C) 10 μM TR_1C, 10 μM TR_2C, 10 μM MasX, and 10 μM EGTA was mixed with $CaCl_2$. Calcium concentrations of the $CaCl_2$ solutions are shown in the figure. Experimental conditions are the same as in Figure 3. The horizontal solid line represents the initial level.

concentration), each curve of the Trp-fluorescence intensity change was a sum of one rapid decrease and one slow increase. (ii) When the molar ratio was greater than or equal to 5 (high calcium concentration), each curve had one rapid decrease and one slow decrease. The rate constants of the rapid phase were from 443 ± 62 to 495 ± 11 s^{-1} for the calcium concentrations from 5 to 40 μM, and from 667 ± 13 to 778 ± 15 s^{-1} for the calcium concentrations from 50 to 200 μM. The slow process was biphasic, and its rate constants were from 4.46 ± 0.03 to 20.1 ± 0.5 s^{-1} and from 0.882 ± 0.07 to 5.94 ± 0.05 s^{-1} for the calcium concentrations of 5−40 μM, and from 19.9 ± 0.1 to 21.3 ± 0.2 s^{-1} and from 8.27 ± 0.1 to 10.9 ± 0.2 s^{-1} for the calcium concentrations of 50−200 μM. The rate constants of Ca^{2+}-induced complex formation between CaM and MasX scarcely varied at the high calcium concentrations.

The same types of experiments were performed for CaM fragment(s) and MasX (Figure 4). All TR_1C−MasX (10 μM/10 μM) systems containing 10 μM EGTA showed one rapid fluorescence decrease that finished within 40 ms. In the calcium concentrations under 30 μM, a slow fluorescence increase over about 0.1 s was observed (Figure 4, panel A). (It should be noted here that the stopped-flow kinetic process of the Ca^{2+}-induced TR_1C binding to MasX showed the Trp-fluorescence decrease against the fluorescence increase in the static titration experiment shown in Figure 2. This is due to the difference for the detection methods as mentioned under Materials and Methods.) The rapid phase was analyzed by a double exponential curve except for a case of a calcium concentration of 50 μM. In the case of 50 μM calcium, the trace was analyzed by a single exponential curve. The fast rate constants of the rapid phase were 352 ± 37 to 684 ± 20 s^{-1} for the calcium concentrations of 5−50 μM; the slow rate constants of the rapid phase were 37.2 ± 1.5 to 96.2 ± 64.4 s^{-1} for the calcium concentrations of 5−40 μM. These results indicate that the Ca^{2+}-induced complex formation of TR_1C and MasX is a rapid process of the fluorescence decrease that finishes within 40 ms. As will be shown in a later section, the slow fluorescence increase phase over about 0.1 s in the calcium concentrations under 30 μM is due to the Ca^{2+} transfer from TR_1C to EGTA. The rate constants of the slow process were 1.94 ± 0.1 to 3.77 ± 0.2 s^{-1} for the calcium concentrations of 5−20 μM.

In the TR_2C−MasX (10 μM/10 μM) system containing 10 μM EGTA, the reaction traces were observed as one slow fluorescence increase (Figure 4, panel B). The experimental traces were analyzed by double exponential curves. The fast

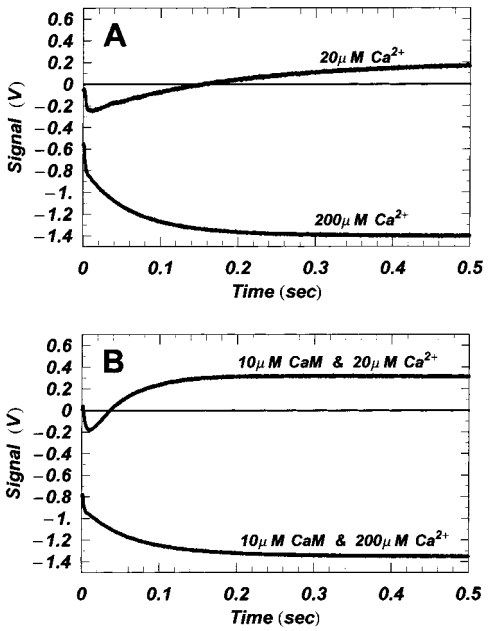

FIGURE 5: Comparison of stopped-flow traces for (A) the Ca^{2+}-induced binding of CaM and MasX and (B) the binding of MasX and Ca^{2+}-bound CaM. Experimental data of panel A are from Figure 3. Stopped-flow traces of panel B were obtained by mixing a solution of 10 μM MasX and 10 μM EGTA with a solution of 10 μM CaM containing 20 or 200 μM $CaCl_2$. Experimental conditions are the same as in Figure 3. The horizontal solid line represents the initial level.

rate constants were 14.1 ± 1.1, 47.1 ± 0.8, and 132 ± 9 s^{-1} for the calcium concentrations of 5, 20, and 50 μM, respectively, and the slow rate constants were 0.753 ± 0.1 to 32.6 ± 2.6 s^{-1}. The Ca^{2+}-induced complex formation of TR_2C and MasX is a slow biphasic process, and the reaction due to Ca^{2+} transfer from TR_2C to EGTA was not observed as an independent phase.

When calcium was mixed with the TR_1C-TR_2C-MasX (10 μM/10 μM/10 μM) system containing 10 μM EGTA, all reaction traces were always observed as one rapid fluorescent decrease and one slow increase (Figure 4, panel C). The rate constants of the rapid phase were 216 ± 20 to 632 ± 51 s^{-1} for the calcium concentrations of 10−50 μM. For the calcium concentration 5 μM, the rapid phase could not be analyzed exactly because the amplitude of this phase was too small. The slow process was biphasic, and its rate constants of the fast phase were 1.86 ± 0.1, 9.85 ± 0.3, and 115 ± 6 s^{-1} for the calcium concentrations of 5, 20, and 50 μM, respectively, and those of the slow phase were 0.361 ± 0.05, 7.49 ± 0.2, and 9.36 ± 0.07 s^{-1} for the calcium concentrations of 5, 30, and 50 μM, respectively. Compared with the results of the TR_1C-MasX and TR_2C-MasX systems, the fast and slow processes of the TR_1C-TR_2C-MasX system represent the Ca^{2+}-induced MasX binding of TR_1C and TR_2C, respectively.

We performed another type of experiment in which MasX (10 μM) containing 10 μM EGTA was mixed with Ca^{2+}-bound CaM (10 μM) (MasX versus Ca^{2+}-CaM system) and the stopped-flow traces for this system were observed (Figure 5, panel B). These traces were mostly similar to that of the CaM−MasX versus Ca^{2+} system (CaM−MasX system) (Figure 5, panel A). At the high calcium concentrations from 50 to 200 μM for both systems, the rate constants of the

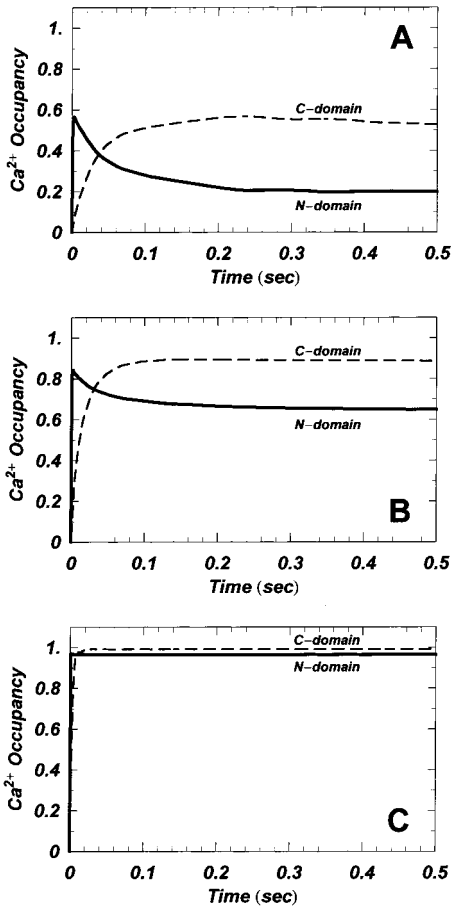

FIGURE 6: Simulations of time-courses of the Ca^{2+} occupancies of the N- and C-domains of CaM. The initial Ca^{2+} concentration at time zero is (A) 10 μM, (B) 25 μM, and (C) 100 μM in a solution of 5.0 μM CaM containing 5.0 μM EGTA. The thick and dashed lines represent the Ca^{2+} occupancies of the N- and C-domains of CaM, respectively.

rapid phase were in the range from 667 ± 13 to 847 ± 26 s^{-1}, while the fast phase of the slow biphasic process had a constant rate of 20.3 ± 1.0 s^{-1} independent of the calcium concentrations. The slow rate constants of the slow process of the MasX versus Ca^{2+}-CaM system were around 2.80 ± 1.3 s^{-1} at the calcium concentrations over 100 μM. These values were lower than those for the CaM−MasX system. On the other hand, at the low calcium concentrations of 5−40 μM, the rate constants of the rapid fluorescence decrease process of the MasX versus Ca^{2+}-CaM system (220 ± 3.5 to 495 ± 64 s^{-1}) are similar to those of the CaM−MasX system. The slow fluorescence increase phases were analyzed by a single exponential curve, and these rate constants had a constant value of 19.8 ± 2.0 s^{-1} independent of the calcium concentrations. This value is larger than most of those of the CaM−MasX system at the low calcium concentrations. These results indicate that the rapid and slow processes of this system also represent the MasX binding of the N- and C-domains of CaM, respectively.

Numerical Simulations for Ca^{2+} Binding of Each Domain of CaM. We simulated the time-course of Ca^{2+} binding to each domain of CaM. Figure 6 shows time-courses of the Ca^{2+} occupancies of the Ca^{2+}-binding sites within the N- and C-domains of CaM when the calcium concentration is jumped, at time zero, from zero to a finite value in a solution of 5.0 μM CaM containing 5.0 μM EGTA.

In Figure 6, panels A and B show that the Ca^{2+} occupancy of the N-domain increased rapidly during the time range of 2 ms, and then decreased gradually. In contrast, the Ca^{2+} occupancy of the C-domain increased gradually and reached a peak at around about 0.25 s (panel A) and 0.1 s (panel B), respectively. Then this Ca^{2+} occupancy decreased very slowly. These Ca^{2+} occupancy curves of the N- and C-domains by about 0.25 s reflect the differences in the static and kinetic properties of the N- and C-sites. The Ca^{2+} affinity of the N-sites is lower than the C-sites, while the Ca^{2+}-binding or Ca^{2+}-removal reaction of the N-sites is faster than the C-sites (*70*). In the time range of 2 ms−0.25 s, Ca^{2+} transfer from the N-domain to the C-domain occurs, causing the Ca^{2+} occupancies of both domains to change as shown in panels A and B of Figure 6. The same behavior has been suggested by the other reports (*44*, *64*). At the long time range over 0.5 s, the Ca^{2+} occupancies of both the N- and C-domains decreased gradually and leveled off by about 1 and 2.5 s, respectively. These gradual changes were due to the Ca^{2+} transfer to EGTA. When Ca^{2+} concentration was high, the Ca^{2+} occupancies of both domains increased rapidly and leveled off by about 20 ms (Figure 6, panel C). Thus, little Ca^{2+} transferred from the N- and C-domains to EGTA. These traces of the Ca^{2+} occupancies of the N- and C-domains could be approximated by triple to double exponential curves and double to single exponential curves, respectively. The increase phase of the Ca^{2+} occupancy of the N-domain has the high rate constants of 950, 1900, 4700, and 13 100 s^{-1} for the calcium concentrations of 2.5, 10, 25, and 100 μM, respectively. These rate constants were much higher than those of the experimentally observed rapid processes of the $TR_1C-TR_2C-MasX$, CaM−MasX, and MasX versus Ca^{2+}-CaM systems. The decrease phase of the Ca^{2+} occupancy of the N-domain was biphasic due to the Ca^{2+} transfer to the C-domain and EGTA. The rate constants were between 20 and 33 s^{-1} for the calcium concentrations of 2.5−50 μM and between 0.08 and 2.8 s^{-1} for the calcium concentrations of 2.5−25 μM. On the other hand, the increase phase of the Ca^{2+} occupancy of the C-domain has the rate constants of 50, 58, 95, and 470 s^{-1} for the calcium concentrations of 2.5, 10, 25, and 100 μM, respectively. These rate constants were similar to or higher than those of the experimentally observed fast phases of the slow processes of the $TR_1C-TR_2C-MasX$, CaM−MasX, and MasX versus Ca^{2+}-CaM systems. And the decrease phase of the Ca^{2+} occupancy of the C-domain, which was due to the Ca^{2+} transfer to EGTA, had the rate constants of 0.9−5.3 s^{-1} for the calcium concentrations of 2.5−37.5 μM.

We also simulated the Ca^{2+} binding of an isolated single domain or fragment under similar conditions. The Ca^{2+} binding of the single N-domain proceeded at high speed, and this Ca^{2+} occupancy peaked at about 2 ms, and then decreased gradually due to the Ca^{2+} transfer to EGTA. The rate constants of the former change of the Ca^{2+} occupancy were 2200−3800 s^{-1} for the calcium concentrations of 2.5−25 μM, while those of the latter change were 1.6−15 s^{-1}. These fast rate constants of the rapid reaction are much higher than those of the experimentally observed rapid process of the $TR_1C-MasX$ system, indicating that Ca^{2+} binding of the single N-domain induces subsequent MasX binding of Ca^{2+}-bound N-domain. The slow Ca^{2+} transfer from the single N-domain to EGTA was observed in the stopped-flow experiment for the $TR_1C-MasX$ system (the upper trace in panel A of Figure 4). The simulation traces of the Ca^{2+} binding of the single C-domain were composed of one rapid increase, which reached a peak at about 0.1 s, and one slow decrease due to the Ca^{2+} transfer to EGTA. The rate constants of the former change of the Ca^{2+} occupancy were 53−105 s^{-1} for the calcium concentrations of 2.5−25 μM, while those of the latter change were 0.87−8.5 s^{-1}. These fast rate constants of the single C-domain were in the range of the fast rate constants of the slow biphasic process observed experimentally in the $TR_2C-MasX$ system. On the other hand, the higher the calcium concentration, the smaller the amplitudes of the slow change of both single domains became. These mean less occurrence of the Ca^{2+} transfer from the single N- or C-domains to EGTA.

DISCUSSION

MasX Binding of CaM and CaM Tryptic Fragments, TR_1C and TR_2C. We can deduce the state of the complex of CaM or CaM fragment(s) and MasX from the fluorescence anisotropy experiments. In the presence of calcium, the fluorescence anisotropy titration curve of MasX with an equimolar mixture of TR_1C and TR_2C (TR_1C-TR_2C system) showed a steep increase at lower molar ratio of the fragments to MasX ($[TR_1C-TR_2C]/[MasX] < 1$) and saturation at a 1:1 molar ratio of each fragment to MasX (Figure 1, panel B). This means that the final product of the titration is either a mixture of $TR_1C-MasX$ complex and $TR_2C-MasX$ complex (competitive binding) or a 1:1:1 complex of TR_1C, TR_2C, and MasX (independent binding). But the result of this experiment alone cannot lead us to determine the final state of the complex. So we considered how two kinds of binding resulted in fluorescence titration with calcium, and compared the results with the experimental data of the $TR_1C-TR_2C-MasX$ system. If MasX binding of the TR_1C-TR_2C system were competitive, the titration curve would be the summation of the experimental titration curves of the $TR_1C-MasX$ and $TR_2C-MasX$ systems. And the $pCa_{1/2}$ of the curve would be an average of $pCa_{1/2}$s of both systems. But the experimental $pCa_{1/2}$ of this $TR_1C-TR_2C-MasX$ system is larger than that of the $TR_2C-MasX$ system, indicating that the complex for the TR_1C-TR_2C system is a 1:1:1 complex of TR_1C, TR_2C, and MasX (independent binding).

Panel A of Figure 1 shows that CaM binds MasX strongly at a 1:1 stoichiometry in the presence of calcium. But this result alone does not determine whether either or both of the two domains of CaM bind to MasX. The fluorescence titration curve of Figure 2 determines the state of the complex. The titration curve of the CaM−MasX system has a three-state transition. Comparing the titration curve of the CaM−MasX system with those of the $TR_1C-MasX$ and $TR_2C-MasX$ systems, we can conclude that the transition of the titration curve of the CaM−MasX system at the high-pCa region is clearly due to the Ca^{2+}-induced binding of the C-domain of CaM to MasX, resulting in the formation of a static intermediate. The transition at the low-pCa region is due to the Ca^{2+}-induced binding of the N-domain of CaM to MasX, leading the complex to a final product in which MasX binds both the N- and C-domains of CaM. Since both domains can bind MasX in the presence of calcium, the linear increase of the anisotropy at the low CaM concentrations

([CaM]/[MasX] < 1) in the presence of calcium means that both Ca^{2+}-bound domains of CaM bind cooperatively to MasX (*62*).

Thus, we revealed that the N- and C-domains of CaM, which were connected by the central linker, bound cooperatively to MasX in the presence of calcium. On the other hand, TR_1C and TR_2C bound independently to MasX. The central linker of CaM plays an important role in the cooperative binding of both domains to MasX. In other words, the cooperative interaction between the N- and C-domains of CaM through the central linker results in the cooperative binding of both the domains to MasX. Another reason for the cooperative binding of both the domains is the following: When one of the domains of CaM binds to MasX, the other domain is less than 6.5 nm apart from the MasX molecule, so that this situation is equivalent to that the concentration of the other domain around MasX is higher than 1.4 mM (*22*, *71*). This value is so high that the other domain also binds to the MasX molecule.

In the absence of calcium, the fluorescence anisotropy titration of the CaM, TR_2C, and TR_1C-TR_2C systems resulted in no saturation, while the TR_1C system showed little change of the anisotropy. These experimental results suggest that in the absence of calcium the C-domain of CaM interacts weakly with MasX and the N-domain does not. The weak interaction between the C-domain of CaM and MasX may be due to the electrostatic interaction (*36*).

Our *K*d values are higher than the values reported by the other groups (*47*, *57*, *58*, *72*). Although there are differences in the experimental conditions between ours and the other groups, we are not certain why these *K*d values were different. However, it is certain that the Ca^{2+} binding to CaM induces strong binding of the Ca^{2+}-bound CaM to MasX.

Kinetics of Ca^{2+}-Induced CaM or CaM Fragment(s) Binding to MasX. We found in this kinetic study that the reaction traces of the Ca^{2+}-induced complex formation of CaM and MasX varied with the calcium concentrations of the calcium solutions as shown in Figure 3. Before discussing the details of the reaction traces of Figure 3, we discuss at first the simple cases of the CaM fragment(s) and MasX systems.

The TR_1C-MasX system showed a rapid process of fluorescence decrease, which finished within 40 ms, at all calcium concentrations of 5−50 μM and a slow process of fluorescence increase over about 0.1 s at the calcium concentrations under 30 μM (Figure 4, panel A). The rapid process of the TR_1C-MasX system was biphasic. The fast phase of the rapid process had the high rate constants of 352−684 s^{-1}. The numerical simulation revealed that the Ca^{2+} binding of the single N-domain had rate constants higher than 2000 s^{-1}. So the fast phase of the rapid process is the MasX binding of the Ca^{2+}-bound TR_1C that follows the rapid Ca^{2+} binding of TR_1C, while the slow phase of the rapid process (rates 37.2−96.2 s^{-1}) would be a rearrangement of the structure of the TR_1C-MasX complex. In contrast, the slow process of the TR_1C-MasX system is due to the Ca^{2+} transfer from TR_1C to EGTA because of the following: (i) the sign of the amplitude of the slow process of the experimental trace was reversed to that of the rapid process; this slow experimental trace was the same as the result of the numerical simulation; and (ii) this slow process did not appear at the high calcium concentrations of 30 μM and greater enough for calcium to bind fully to TR_1C (10 μM), which has two Ca^{2+}-binding sites, and EGTA (10 μM).

In the TR_2C-MasX system, the reaction traces were slow biphasic processes of one fluorescence increase (Figure 4, panel B). The fast phase of the slow process had the rate constants of 14.1−132 s^{-1} at the calcium concentrations of 5−50 μM. These rate constants were similar to the Ca^{2+}-binding rates of the single C-domain obtained by the numerical simulation (53−105 s^{-1}). So the fast phase of the slow process of the TR_2C-MasX system represents the simultaneous reactions of the Ca^{2+} binding of TR_2C and the MasX binding of the Ca^{2+}-bound TR_2C. Although the slow phase of the slow process had the rate constants of 0.753−32.6 s^{-1}, similar to those of the Ca^{2+} transfer from the single C-domain to EGTA obtained by the numerical simulation (0.87−8.5 s^{-1}), the sign of the amplitude of the slow phase of the fluorescence change was the same as that of the fast phase. Therefore, we can conclude that the slow phase of the TR_2C-MasX system does not represent the Ca^{2+} transfer from TR_2C to EGTA. It represents another reaction, such as the structural rearrangement of the TR_2C-MasX complex.

Stopped-flow traces of the TR_1C-TR_2C-MasX system had one rapid fluorescence decrease and one slow fluorescence increase (Figure 4, panel C). The rate constants of the rapid fluorescence decrease of the TR_1C-TR_2C-MasX system (216−632 s^{-1} at the calcium concentrations of 10−50 μM) were similar to the fast rate constants of the rapid process observed for the TR_1C-MasX system (Figure 4, panel A; rates 352−684 s^{-1} at the calcium concentrations of 5−50 μM). The rapid process, therefore, indicates the MasX binding of the Ca^{2+}-bound TR_1C. On the other hand, the slow process of the TR_1C-TR_2C-MasX system showed one slow biphasic fluorescence increase similar to the stopped-flow trace of the TR_2C-MasX system (Figure 4, panel B). But the rate constants of the fast phase of the slow process of the TR_1C-TR_2C-MasX system (1.86, 9.85, and 115 s^{-1} at the calcium concentrations of 5, 20, and 50 μM, respectively) are lower than those of the TR_2C-MasX system (14.1, 47.1, and 132 s^{-1} at the calcium concentrations of 5, 20, and 50 μM, respectively). In particular, these rate constants of the TR_1C-TR_2C-MasX and TR_2C-MasX systems showed a large difference at the low calcium concentration. The rate constants of the TR_1C-TR_2C-MasX system for the low calcium concentrations are also lower than those of the increase phase of the Ca^{2+} occupancy trace of the C-domain for the low calcium concentrations in the numerical simulation of the coexisting N- and C-domains (Figure 6; rates 50, 58, 95, and 470 s^{-1} for the calcium concentrations of 2.5, 10, 25, and 100 μM, respectively). These would be due to rapid decreases of both the free Ca^{2+} concentration and the free MasX concentration, which were induced by the rapid Ca^{2+} binding and MasX binding of TR_1C in the TR_1C-TR_2C-MasX system. These rapid decreases result in the slower Ca^{2+}-binding reaction of TR_2C and the simultaneous slower binding of Ca^{2+}-bound TR_2C to MasX in the TR_1C-TR_2C-MasX system compared to the TR_2C-MasX system at the same calcium concentration. If the calcium concentration is not enough to bind fully to the whole Ca^{2+}-binding sites of the N- and C-domains, some of the Ca^{2+} ions that bound to the N-sites by the rapid binding reaction transfer gradually to the C-sites (Figure 6), because

the Ca^{2+} affinity of the N-sites is lower than that of the C-sites, while the Ca^{2+}-binding rate of the N-sites is much faster than that of the C-sites. This Ca^{2+} transfer from the N-sites to the C-sites induces a removal of the N-domain from MasX and a binding of the C-domain to MasX. These processes result in the slow fluorescence increase at the second stage in the $TR_1C-TR_2C-MasX$ system. The slow process is biphasic. The fast phase of the slow process is due to the Ca^{2+}-induced binding of TR_2C to MasX, and the slow phase of the slow process may be due to a rearrangement of the complex structure.

Since the rate constants of the rapid reaction of the CaM−MasX system are similar to those of the Ca^{2+}-induced binding of TR_1C to MasX and are lower than those of the Ca^{2+} binding of the N-domain obtained by the numerical simulation of the coexisting N- and C-domains, we can conclude that the rapid process of the fluorescence decrease observed for the CaM−MasX system was due to the Ca^{2+}-induced N-domain binding to MasX that follows the rapid Ca^{2+} binding of the N-domain. The rate constants of this process were 443−495 s^{-1} at the calcium concentrations of 5−40 μM and 667−778 s^{-1} at the calcium concentrations of 50−200 μM.

The slow process of the fluorescence increase or decrease observed for the CaM−MasX system, which varied with the calcium concentrations, represents the Ca^{2+}-induced binding between the C-domain of CaM and MasX. At the low calcium concentrations of 5−40 μM, the CaM−MasX system showed the reaction traces with one rapid fluorescence decrease and one slow increase (Figure 3, traces 1−5). These stopped-flow traces are similar to those of the $TR_1C-TR_2C-MasX$ system (Figure 4, panel C). At the high calcium concentrations of 50−200 μM, we observed the slow biphasic fluorescence decrease after the rapid fluorescence decrease (Figure 3, traces 6−10). These traces are different from those observed for the $TR_1C-TR_2C-MasX$ system. This difference at the high calcium concentrations can be explained by the different binding schemes for the CaM−MasX system and the $TR_1C-TR_2C-MasX$ system: the cooperative binding of both domains of CaM for the CaM−MasX system and the independent binding of the tryptic fragments for the $TR_1C-TR_2C-MasX$ system. The N- and C-domains of CaM are connected with the central linker of CaM. The slow fluorescence decrease process in the CaM−MasX system represents the binding of the Ca^{2+}-bound C-domain of CaM to MasX that has already bound the Ca^{2+}-bound N-domain. In the final product, CaM may assume a jack-knifed shape. The remarkable difference between the CaM−MasX system and the $TR_1C-TR_2C-MasX$ system is in the rate constant of the fast phase of the slow biphasic process. Even if the calcium concentration increased higher than 100 μM, the rate constants of the fast phase of the slow biphasic process of the CaM−MasX system kept a constant value around 20 s^{-1}. In contrast, the fast rate constant of the slow process (MasX binding of Ca^{2+}-bound TR_2C) of the $TR_1C-TR_2C-MasX$ system increased over 100 s^{-1} as the calcium concentration increased more than 40 μM. These results mean that the Ca^{2+}-induced binding of the C-domain of CaM to MasX has a rate-limiting step. The slow phase of the slow process would be a structural rearrangement in the final CaM−MasX complex, in which MasX binds both domains of CaM. The whole Ca^{2+}-induced complex formation of the CaM−MasX system takes a constant time (around 0.3 s) even if the calcium concentration increases.

As for the MasX versus Ca^{2+}-CaM system, the stopped-flow traces resemble those of the Ca^{2+}-induced binding of CaM and MasX (Figure 5). Stopped-flow traces of the MasX versus Ca^{2+}-CaM system at high calcium concentration, such as 200 μM, represent the binding of MasX and both Ca^{2+}-bound domains of CaM. The rapid fluorescence decrease shows the binding of the Ca^{2+}-bound N-domain of CaM to MasX, and the slow fluorescence decrease shows the binding between the Ca^{2+}-bound C-domain of CaM and MasX, which had already bound to the N-domain. The slow process is biphasic. The rate constants of the fast phase of the slow process have a constant value around 20 s^{-1}. This result also means that the binding process of the Ca^{2+}-bound C-domain of CaM to MasX, which binds already the Ca^{2+}-bound N-domain, has the rate-limiting step with the rate around 20 s^{-1}. The slow phase of the slow process had the rate constants lower than those of the CaM−MasX system, and may represent the slow rearrangement of the CaM−MasX complex.

At a low calcium concentration such as 20 μM, the Ca^{2+} occupancy of the N-sites of CaM is 0.29, and that of the C-sites is 0.63 before the Ca^{2+}-bound CaM is mixed with MasX. (These Ca^{2+} occupancies were calculated from the Kd_{Ca} values described under Materials and Methods.) The rapid fluorescence decrease process represents the rapid binding of the Ca^{2+}-bound N-domain of CaM to free MasX. The slow fluorescence increase process shows a sum of the slow binding reactions of the Ca^{2+}-bound C-domain of CaM to both free MasX and MasX that had rapidly bound to the Ca^{2+}-bound N-domain. This slow process was observed in this experiment as a single phase with the rate constant around 20 s^{-1}. Therefore, the binding reaction between the Ca^{2+}-bound C-domain of CaM and MasX proceeds at the maximal rate constant of around 20 s^{-1}. The Ca^{2+} transfer from the N-sites of CaM to the C-sites does not occur in this system.

Summarized, we revealed in this study that the rapid Ca^{2+} binding of TR_1C induced the resultant binding of Ca^{2+}-bound TR_1C to MasX, while the slow Ca^{2+} binding of TR_2C and the binding of Ca^{2+}-bound TR_2C to MasX proceeded simultaneously. The Ca^{2+}-induced complex formation of the $TR_1C-TR_2C-MasX$ system is a sum of independent reactions of the $TR_1C-MasX$ and $TR_2C-MasX$ systems. In the Ca^{2+}-induced binding of CaM to MasX, the rapid Ca^{2+}-binding-induced N-domain binding to MasX precedes the binding of the slow Ca^{2+}-bound C-domain to MasX. The C-domain of CaM is connected to the N-domain by the central linker, and the binding of the C-domain to MasX occurs at the maximal rate constant of around 20 s^{-1}. This result means that the binding process of the C-domain of CaM to MasX has a rate-limiting step; that is, the central linker of CaM regulates the C-domain binding to MasX. This rate-limiting step is characteristic of the cooperative binding reaction of both domains of CaM to MasX, and would represent the bending of the flexible central linker of CaM for CaM to assume a jack-knifed shape around MasX.

Reaction Scheme for Ca^{2+}-Induced Complex Formation between CaM and MasX. On the basis of our experimental results, we can describe the Ca^{2+}-induced CaM binding to MasX using the kinetic scheme of Figure 7. The Ca^{2+}-

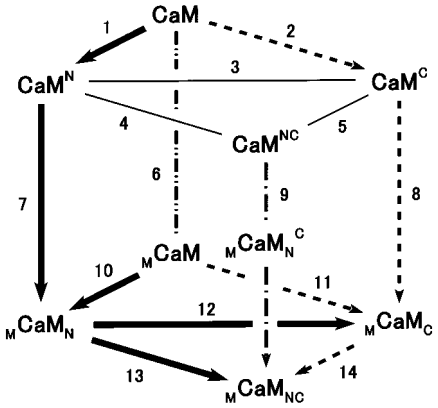

FIGURE 7: Kinetic scheme of complex formation between CaM, MasX, and Ca^{2+}. The abbreviations are as follows: CaM, apoCaM; CaM^N, CaM with the Ca^{2+}-bound N-domain; CaM^C, CaM with the Ca^{2+}-bound C-domain; CaM^{NC}, CaM with the Ca^{2+}-bound N- and C-domains; ${}_MCaM$, MasX complex with apoCaM; ${}_MCaM_N$, MasX complex with the Ca^{2+}-bound N-domain of CaM; ${}_MCaM_C$, MasX complex with the Ca^{2+}-bound C-domain of CaM; ${}_MCaM_{NC}$, MasX complex with the Ca^{2+}-bound N- and C-domains of CaM; ${}_MCaM_N^C$, MasX complex with the N-domain of full Ca^{2+}-bound CaM. The thick arrows are the kinetic routes of the Ca^{2+}-induced complex formation between CaM and MasX; the dashed arrows, the Ca^{2+}-induced complex formation between CaM and MasX in the static calcium titration experiment; the dash−dotted arrow (route 9), the kinetic route of the complex formation between full Ca^{2+}-bound CaM and MasX. The dash−dot−dotted line (route 6) represents the equilibrium between apoCaM and apoCaM−MasX complex. The other lines represent the equilibrium between species. The numbers are explained in the text.

induced CaM binding to MasX proceeds mainly through routes 1, 7, and 12 at the low calcium concentration. When the calcium concentration is high, the main route is through routes 1, 7, and 13. Routes 1, 7, and 10 are rapid processes, and routes 12 and 13 are slow processes. Route 7 shows the rapid fluorescence decrease in the stopped-flow experiments; routes 12 and 13 show the slow fluorescence increase and decrease, respectively. Route 13 has a rate-limiting step, whose rate constant is around 20 s^{-1}. In the calcium titration experiment, the CaM−MasX complex is formed mainly through routes 2, 8, and 14. Route 8 shows the fluorescence increase in the fluorescence titration experiment, and route 14 shows the fluorescence decrease. These routes have been suggested by other groups using different target peptides (*46*, *48*, *49*, *52*). Our experimental results support their suggestions.

When Ca^{2+}-bound CaM was mixed with MasX, four species of CaM, that is, CaM, CaM^N, CaM^C, and CaM^{NC}, bind MasX and produce ${}_MCaM$, ${}_MCaM_N$, ${}_MCaM_C$, and ${}_MCaM_{NC}$ through routes 6, 7, 8, and 9, respectively. Route 8 shows the slow process of the fluorescence increase, and route 9 shows the rapid fluorescence decrease and the slow decrease that has the rate-limiting step mentioned above. Route 6 shows little fluorescence intensity change. The distribution of the four species of CaM depends on the calcium concentration, and can be calculated using the Kd_{Ca} values of the N- and C-sites. For example, the [CaM]:[CaM^N]:[CaM^C]:[CaM^{NC}] is 0.26:0.11:0.45:0.18 when the system contains 20 μM calcium, and 0:0:0.02:0.98 when total calcium concentration is 200 μM, respectively. Since the CaM^C fraction is larger than the CaM^{NC} fraction at the calcium concentration of 20 μM, the observed reaction is the trace with one rapid fluorescence decrease and one slow increase. At the higher calcium concentration, the reaction proceeds through route 9 in which the complex forms ${}_MCaM_N^C$ as a kinetic intermediate, so that the trace with one rapid fluorescence decrease and one slow decrease is observed. This molecular kinetic mechanism of Ca^{2+}-induced CaM binding to MasX can explain our experimental data.

On the basis of this molecular kinetic mechanism, the behavior of CaM in the cell can be described as follows: when the Ca^{2+} concentration in the cell increases rapidly, the N-domain of CaM responds to the Ca^{2+} concentration change and binds Ca^{2+} faster than the C-domain of CaM. The other Ca^{2+}-binding proteins such as phospholipase A_2 and protein kinase C bind Ca^{2+} slower than CaM (*73*). The Ca^{2+}-bound N-domain of CaM binds rapidly the target protein. Then the Ca^{2+}-bound C-domain of CaM binds slowly and tightly the target protein, and activates it.

We examined finally what structure the full Ca^{2+}-bound CaM complex with MasX assumed at the final equilibrium state on the basis of our static studies and the other reports (*26*, *28*, *29*, *38*, *58*, *59*, *72*, *74*, *75*). In the experiments of the fluorescence spectroscopy, we observed the blue-shift of the Trp emission peak of MasX from about 350 nm to about 330 nm, which is induced by CaM or fragment(s) binding of MasX (*58*). These observations mean that the Trp residue of MasX is close to the hydrophobic part of each domain of CaM. In addition, the calcium titration curve of the CaM−MasX system resulted in a three-state transition. This is different from that of the CaM−MLCK peptide system that showed a two-state transition (*38*). The structure of the CaM−MLCK peptide complex has been solved (*26*, *28*). According to the structure, CaM takes a jack-knifed shape around the MLCK peptide and the Trp residue of the MLCK peptide is buried around the hydrophobic part of the C-domain of CaM. Moreover, Osawa et al. reported the determination for the peptide-binding direction in the CaM complex, in which eight acidic residues of a channel that is formed by helix I of the N-domain and helices VI, VII, and VIII of the C-domain of CaM are close to the basic cluster of the Lys and Arg residues of the target peptide (*29*). In the CaM−MLCK peptide complex, this channel of CaM is close to the basic cluster at the N-terminal of the MLCK peptide, resulting in an antiparallel structure. On the basis of these characteristics, we think the CaM−MasX complex is as follows: In the MasX molecule, the basic cluster that is composed of Lys 11 and Lys 12 is located at the C-terminal of MasX. This location of the basic cluster of MasX suggests that the CaM−MasX complex assumes a parallel structure. So the environment of Trp in the CaM−MasX complex would be different from that in the CaM−MLCK peptide complex. The remarkable Trp-fluorescence decrease in our experiment of the CaM−MasX system would be due to the structural effect on the Trp chromophore of MasX, such as quenching, in the CaM−MasX complex (*59*, *72*, *74*, *75*). We assumed here that in the CaM−MasX complex CaM took a jack-knifed structure around MasX (*63*). But we cannot rule out the possibility that the CaM−MasX complex assumes the other type of structure.

Conclusion. In this study, we revealed a molecular kinetic mechanism of the Ca^{2+}-induced CaM binding to MasX. At first, rapid Ca^{2+} binding to the N-domain of CaM induces the resultant binding of MasX to this domain. This step

allows the C-domain of CaM to be close to the MasX molecule. Although the binding of Ca^{2+} to the C-domain of CaM is a relatively slow process, the Ca^{2+}-binding process of the C-domain, which has high affinity for Ca^{2+} and MasX, induces the binding of the C-domain to MasX through the rate-limiting step, forming the stable product of CaM and MasX. The flexible central linker of CaM induces the cooperative binding of both domains of CaM to MasX in the presence of calcium. The fast N-domain binding and strong C-domain binding of CaM to target protein(s) are very important and effective for the physiological function of CaM.

ACKNOWLEDGMENT

We gratefully acknowledge Drs. Tsutomu Kouyama (Nagoya University, Nagoya, Japan), Michio Yazawa (Hokkaido University, Sapporo, Japan), and Peter M. Bayley (National Institute for Medical Research, London, U.K.) for their helpful advice and encouragement in this study.

REFERENCES

1. Klee, C. B., Crouch, T. H., and Richman, P. G. (1980) *Annu. Rev. Biochem. 49*, 489−515.
2. Means, A. R., and Dedman, J. R. (1980) *Nature 285*, 73−77.
3. Kretsinger, R. H. (1979) *Adv. Cyclic Nucleotide Res. 11*, 1−26.
4. Berridge, M. J., Bootman, M. D., and Lipp, P. (1998) *Nature 395*, 645−648.
5. Trewavas, A. J., and Malho, R. (1998) *Curr. Opin. Plant Biol. 1*, 428−433.
6. Williams, R. J. (1998) *Biochim. Biophys. Acta 1448*, 153−165.
7. Carafoli, E., and Klee, C., Eds. (1999) in *Calcium as a Cellular Regulator*, Oxford University Press, New York.
8. Cheung, W. Y. (1980) *Science 207*, 19−27.
9. Kennedy, M. B. (1989) *Trends Neurosci. 12*, 417−420.
10. Chakravarthy, B., Morley, P., and Whitfield, J. (1999) *Trends Neurosci. 22*, 12−16.
11. Chin, D., and Means, A. R. (2000) *Trends Cell Biol. 10*, 322−328.
12. Hinrichsen, R. D. (1993) *Biochim. Biophys. Acta 1155*, 277−293.
13. Jurado, L. A., Chockalingam, P. S., and Jarrett, H. W. (1999) *Physiol. Rev. 79*, 661−682.
14. Hook, S. S., and Means, A. R. (2001) *Annu. Rev. Pharmacol. Toxicol. 41*, 471−505.
15. Wolenski, J. S. (1995) *Trends Cell Biol. 5*, 310−316.
16. Saimi, Y., and Kung, C. (1994) *FEBS Lett. 350*, 155−158.
17. Xia, Z., and Storm, D. R. (1997) *Curr. Opin. Neurobiol. 7*, 391−396.
18. Bachs, O., Agell, N., and Carafoli, E. (1992) *Biochim. Biophys. Acta 1113*, 259−270.
19. Lu, K. P., and Means, A. R. (1993) *Endocr. Rev. 14*, 40−58.
20. Gnegy, M. E. (1993) *Annu. Rev. Pharmacol. Toxicol. 32*, 45−70.
21. Babu, Y. S., Bugg, C. E., and Cook, W. J. (1988) *J. Mol. Biol. 204*, 191−204.
22. Crivici, A., and Ikura, M. (1995) *Annu. Rev. Biophys. Biomol. Struct. 24*, 85−116.
23. Persechini, A., Moncrief, N. D., and Kretsinger, R. H. (1989) *Trends Neurosci. 12*, 462−467.
24. Rhoads, A. R., and Friedberg, F. (1997) *FASEB J. 11*, 331−340.
25. O'Neil, K. T., and DeGrade, W. F. (1990) *Trends Biochem. Sci. 15*, 59−64.
26. Meador, W. E., Means, A. R., and Quiocho, F. A. (1992) *Science 257*, 1251−1255.
27. Meador, W. E., Means, A. R., and Quiocho, F. A. (1993) *Science 262*, 1718−1721.
28. Ikura, M., Clore, G. M., Gronenborn, A. M., Zhu, G., Klee, C. B., and Bax, A. (1992) *Science 256*, 632−638.
29. Osawa, M., Tokumitsu, H., Swindells, M. B., Kurihara, H., Orita, M., Shibanuma, T., Furuya, T., and Ikura, M. (1999) *Nat. Struct. Biol. 8*, 819−824.
30. Wang, E., Zhuang, S., Kordowska, J., Grabarek, Z., and Wang, C. A. (1997) *Biochemistry 36*, 15026−15034.
31. Yuan, T., and Vogel, H. J. (1998) *J. Biol. Chem. 273*, 30328−30335.
32. Elshorst, B., Hennig, M., Forsterling, H., Diener, A., Marcus, M., Schulte, P., Schwalbe, H., Griesinger, C., Krebs, J., Schmid, H., Vorherr, T., and Carafoli, E. (1999) *Biochemistry 38*, 12320−12332.
33. Hayashi, N., Izumi, Y., Titani, K., and Matsushima, N. (2000) *Protein Sci. 9*, 1905−1913.
34. Schumacher, M. A., Rivard, A. F., Bachinger, H. P., and Adelman, J. P. (2001) *Nature 410*, 1120−1124.
35. Tsvetkov, P. O., Protasevich, I. I., Gilli, R., Lafitte, D., Lobachov, V. M., Haiech, J., Briand, C., and Makarov, A. A. (1999) *J. Biol. Chem. 274*, 18161−18164.
36. Hill, T. J., Lafitte, D., Wallace, J. I., Cooper, H. J., Tsvetkov, P. O., and Derrick, P. J. (2000) *Biochemistry 39*, 7284−7290.
37. Rodney, G. G., Moore, C. P., Williams, B. Y., Zhang, J. Z., Krol, J., Pedersen, S. E., and Hamilton, S. L. (2001) *J. Biol. Chem. 276*, 2069−2074.
38. Johnson, J. D., Holroyde, M. J., Crouch, T. H., Solaro, R. J., and Potter, J. D. (1981) *J. Biol. Chem. 256*, 12194−12198.
39. Bayley, P., Ahlstrom, P., Martin, S. R., and Forsen, S. (1984) *Biochem. Biophys. Res. Commun. 120*, 185−191.
40. Martin, S. R., Andersson Teleman, A., Bayley, P. M., Drakenberg, T., and Forsen, S. (1985) *Eur. J. Biochem. 151*, 543−550.
41. Suko, J., Pidlich, J., and Bertel, O. (1985) *Eur. J. Biochem. 153*, 451−457.
42. Suko, J., Wyskovsky, W., Pidlich, J., Hauptner, R., Plank, B., and Hellmann, G. (1986) *Eur. J. Biochem. 159*, 425−434.
43. Bowman, B. F., Peterson, J. A., and Stull, J. T. (1992) *J. Biol. Chem. 267*, 5346−5354.
44. Johnson, J. D., Snyder, C., Walsh, M., and Flynn, M. (1996) *J. Biol. Chem. 271*, 761−767.
45. Persechini, A., White, H. D., and Gansz, K. J. (1996) *J. Biol. Chem. 271*, 62−67.
46. Bayley, P. M., Findlay, W. A., and Martin, S. R. (1996) *Protein Sci. 5*, 1215−1228.
47. Brown, S. E., Martin, S. R., and Bayley, P. M. (1997) *J. Biol. Chem. 272*, 3389−3397.
48. Peersen, O. B., Madsen, T. S., and Falke, J. J. (1997) *Protein Sci. 6*, 794−807.
49. Persechini, A., Yano, K., and Stemmer, P. M. (2000) *J. Biol. Chem. 275*, 4199−4204.
50. Minowa, O., and Yagi, K. (1984) *J. Biochem. 56*, 1175−1182.
51. Linse, S., Helmersson, A., and Forsen, S. (1991) *J. Biol. Chem. 266*, 8050−8054.
52. Sorensen, B. R., Eppel, J. T., and Shea, M. A. (2001) *Biochemistry 40*, 896−903.
53. Higashijima, T., Wakamatsu, K., Takemitsu, M., Fujino, M., Nakajima, T., and Miyazawa, T. (1983) *FEBS Lett. 152*, 227−230.
54. Kusunoki, H., Wakamatsu, K., Sato, K., Miyazawa, T., and Kohno, T. (1998) *Biochemistry 37*, 4782−4790.
55. Gilman, A. G. (1987) *Annu. Rev. Biochem. 56*, 615−649.
56. Higashijima, T., Uzu, S., Nakajima, T., and Ross, E. M. (1988) *J. Biol. Chem. 263*, 6491−6494.
57. Malencik, D. A., and Anderson, S. R. (1983) *Biochem. Biophys. Res. Commun. 114*, 50−56.
58. Malencik, D. A., and Anderson, S. R. (1984) *Biochemistry 23*, 2420−2428.
59. McDowell, L., Sanyal, G., and Prendergast, F. G. (1985) *Biochemistry 24*, 2979−2984.
60. Malencik, D. A., and Anderson, S. R. (1986) *Biochem. Biophys. Res. Commun. 135*, 1050−1057.
61. Cachia, P. J., Van Eyk, J., Ingraham, R. H., McCubbin, W. D., Kay, C. M., and Hodges, R. S. (1986) *Biochemistry 25*, 3553−3562.

62. Yazawa, M., Ikura, M., Hikichi, K., Ying, L., and Yagi, K. (1987) *J. Biol. Chem. 262*, 10951−10954.
63. Matsushima, N., Izumi, Y., Matsuo, T., Yoshino, H., Ueki, T., and Miyake, Y. (1989) *J. Biochem. 105*, 883−887.
64. Ohki, S., Yazawa, M., Yagi, K., and Hikichi, K. (1991) *J. Biochem. 110*, 737−742.
65. Itakura, M., and Iio, T. (1992) *J. Biochem. 112*, 183−191.
66. Watterson, D. M., Harrelson, W. G., Jr., Keller, P. M., Sharief, F., and Vanaman, T. C. (1976) *J. Biol. Chem. 251*, 4501−4513.
67. Watterson, D. M., Sharief, F., and Vanaman, T. C. (1980) *J. Biol. Chem. 255*, 962−975.
68. Slavik, J. (1994) in *Fluorescent Probes in Cellular and Molecular Biology*, CRC Press, Boca Raton, FL.
69. Schwarzenbach, V. G., Senn, H., and Anderegg, G. (1957) *Helv. Chim. Acta 40*, 1886−1900.
70. Murase, T. (1997) in M.S. Thesis (in Japanese), Nagoya University, Nagoya, Japan.
71. Sun, H., and Squier, T. C. (2000) *J. Biol. Chem. 275*, 1731−1738.
72. Sanyal, G., Richard, L. M., Carraway, K. L., III, and Puett, D. (1988) *Biochemistry 27*, 6229−6236.
73. Nalefski, E. A., Wisner, M. A., Chen, J. Z., Sprang, S. R., Fukuda, M., Mikoshiba, K., and Falke, J. J. (2001) *Biochemistry 40*, 3089−3100.
74. Yuan, T., Weljie, A. M., and Vogel, H. J. (1998) *Biochemistry 37*, 3187−3195.
75. Chen, Y., and Barkley, M. D. (1998) *Biochemistry 37*, 9976−9982.

BI011782R